High-resolution ultrasound-modulated optical tomography in biological tissues

Sava Sakadžić and Lihong V. Wang

*Optical Imaging Laboratory, Department of Biomedical Engineering, 3120 TAMU, Texas A&M University,
College Station, Texas 77843-3120*

We present a novel implementation of high-resolution ultrasound-modulated optical tomography that, based on optical contrast, can image several millimeters deep into soft biological tissues. A long-cavity confocal Fabry–Perot interferometer, which provides a large etendue and a short response time, was used to detect the ultrasound-modulated coherent light that traversed the scattering biological tissue. Using 15-MHz ultrasound, we imaged with high-contrast light-absorbing structures placed >3 mm below the surface of chicken breast tissue. The resolution along the axial and the lateral directions with respect to the ultrasound propagation direction was better than 70 and 120 μm, respectively. The resolution can be scaled down further by use of higher ultrasound frequencies. This technology is complementary to other imaging technologies, such as confocal microscopy and optical-coherence tomography, and has the potential for broad biomedical applications.   © 2004 Optical Society of America

OCIS codes: 030.1670, 110.0180, 110.7050, 110.7170, 120.2230, 170.3880.

Great effort has been made in the recent past to develop new imaging modalities based on the optical properties of soft biological tissues in the visible and near-infrared regions. At these wavelengths, radiation is nonionizing and the optical properties of biological tissues are related to the molecular structure, offering potential for the detection of functions and abnormalities.

Ultrasound-modulated optical tomography[1,2] is a hybrid technique that was proposed to provide better resolution for the optical imaging of soft biological tissue by combining ultrasonic resolution and optical contrast. Collective motions of the optical scatterers and periodic changes in the optical index of refraction are generated by ultrasound to produce fluctuations in the intensity of the speckles that are formed by the multiple-scattered light.[3–5] The ultrasound-modulated component of light carries information about the optical properties of tissue from the region of interaction between the optical and ultrasonic waves. However, it is a challenge to detect this modulated component efficiently because of diffused light propagation and uncorrelated phases among individual speckles. Several schemes for detection[2,3,6–14] have been explored. A CCD camera that provides parallel speckle detection[8,9,14] was used to produce a better signal-to-noise ratio than a single square-law detector. To obtain resolution along the ultrasonic axis, several groups of scientists explored various techniques, including an ultrasound frequency sweep,[7] computer tomography,[15] and tracking of ultrasound pulses[11] or short bursts.[13] The pulsed ultrasound approaches provide direct resolution along the ultrasonic axis and are more compatible with conventional ultrasound imaging. Pulsed ultrasound can have a much higher instantaneous power than cw ultrasound, reducing the undesired effect of the increased noise owing to its wide bandwidth.

In this Letter, for the first time to our knowledge, we report high-resolution ultrasound-modulated optical imaging with a long-cavity confocal Fabry–Perot interferometer (CFPI).[16] Our CFPI has a greater etendue—defined as the product of the acceptance solid angle and the area—than most CCD cameras and provides parallel speckle processing. In addition, a CFPI can detect the propagation of high-frequency ultrasound pulses in real time and tolerate speckle decorrelation. A CFPI is especially efficient at high ultrasound frequencies, where the background light can be filtered out effectively while the ultrasound-modulated component is transmitted. With our setup, optical features of ~100 μm in size embedded more than 3 mm below the surface of chicken breast tissue were resolved with high contrast in both the axial and the lateral directions.

The experimental setup is shown in Fig. 1. Samples were gently pressed through a slit along the Z axis to create a semicylindrical bump. The orthogonal ultrasonic and optical beams [Fig. 1(b)] were focused to the same spot below the sample surface. Diffusely transmitted light was collected by an optical fiber with a 600-μm core diameter. This configuration minimized the contribution of unmodulated light from the shallow regions to the background and in addition enhanced the interaction between the ultrasound and some quasi-ballistic light that still existed at small imaging depths (up to one transport mean free path).

A focused ultrasound transducer (Ultran; 15-MHz central frequency, 4.7-mm lens diameter, 4.7-mm focal length, 15-MHz estimated bandwidth) was driven by a pulser (GE Panametrics, 5072PR). The ultrasound focal peak pressure was 3.9 MPa, within the ultrasound safety limit at this frequency for tissues without well-defined gas bodies.[17] The laser light (Coherent, Verdi; 532-nm wavelength) was focused onto a spot of ~100-μm diameter below the surface of an otherwise scatter-free sample. The optical power delivered to the sample was 100 mW. Although the cw power in this proof-of-principle experiment exceeded the
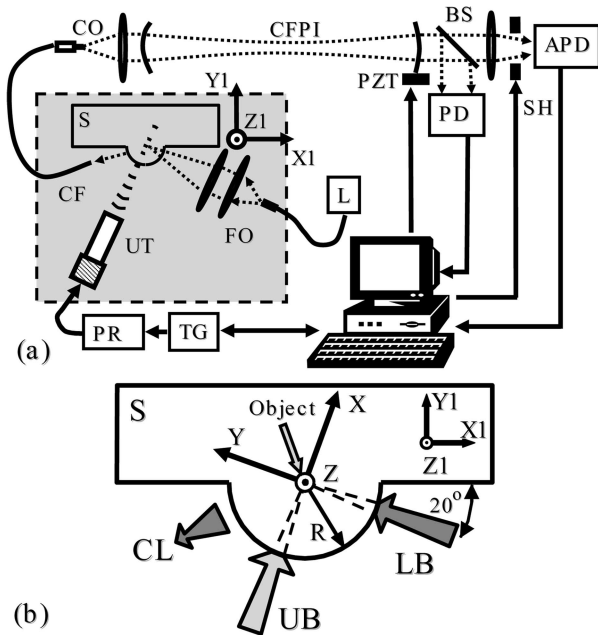
Fig. 1. (a) Schematic of the experimental setup: L, laser; TG, trigger generator; PR, pulser–receiver; UT, ultrasonic transducer; FO, focusing optics; CF, collecting fiber; S, sample; CO, coupling optics; PZT, piezoelectric transducer; BS, beam splitter; SH, shutter; PD, photodetector. (b) Top view of the sample (S): UB, ultrasound beam; LB, incident light beam; CL, collected light; R, radius of curvature. Other abbreviations defined in text.

safety limit for average power, the duration of the sample's exposure to light can be reduced to only a few microseconds for each ultrasound pulse propagation through the region of interest, and therefore the safety limit will not be exceeded in practice even if the focus is maintained in a scattering medium. The sample was mounted on a three-axis ($X1$, $Y1$, and $Z1$) translational stage. The ultrasound transducer and the sample were immersed in water for acoustic coupling. The light-focusing optics and the collecting fiber were immersed in the same water tank. The collected light was coupled into the CFPI, which was operated in a transmission mode (50-cm cavity length, 0.1-mm^2 sr etendue, >20 finesse). The light sampled by the beam splitter was used in a cavity tuning procedure. First we swept the cavity through one free spectral range to find the position of the central frequency of the unmodulated light. Then one CFPI mirror was displaced by a calibrated amount such that the cavity was tuned to the frequency of one sideband of the ultrasound-modulated light (15 MHz greater than the laser light frequency). An avalanche photodiode (APD; Advanced Photonix) acquired the light filtered by the interferometer, and the signal was sampled at 100 Msamples/s with a data acquisition board (Gage, CS14100). A computer program written with LabView software controlled the movement of the CFPI mirror and the other sequences of the control signals.

A trigger generator (Stanford Research, DG535) triggered both ultrasound-pulse generation and data acquisition from the APD. As the resonant frequency

of the CFPI cavity coincided with one sideband of the ultrasound-modulated light, the signal acquired by the APD during the ultrasound propagation through the sample represented the distribution of the ultrasound-modulated optical intensity along the ultrasonic axis and, therefore, yielded a one-dimensional (1D) image. In each operational cycle, first the resonant frequency of the CFPI was tuned and then data from 4000 ultrasound pulses were acquired in 1 s. Averaging over ten cycles was usually necessary to produce a satisfactory signal-to-noise ratio for each 1D image. We obtained two-dimensional images by scanning the sample along the Z direction and acquiring each corresponding 1D image.

Figure 2 presents a typical profile of the temporal dependence of the ultrasound-modulated light intensity during ultrasound-pulse propagation through the sample. The time of propagation was multiplied by 1500 ms^{-1}, the approximate speed of sound in the sample, to be converted into distance along the X axis, where the origin corresponded to the trigger for the signal acquisition from the APD. The sample, made from chicken breast tissue, was pressed through the 4-mm-wide slit. A long rod of 60-μm diameter, made from black latex, which was transparent for ultrasound but absorptive for light, was placed below the sample surface along the Z axis of the cylindrical tissue bump of a 2-mm radius. Because the profiles of the optical radiance and the ultrasound intensity within the sample determined the distribution of the ultrasound-modulated optical intensity, the maximum corresponded to the crossing point between the optical and the ultrasonic axes, as indicated in Fig. 2. The differences between the optical properties of the object and the tissue created a deep dip in the ultrasound-modulated light intensity when the ultrasound pulse passed through the object.

To investigate the axial and lateral resolutions, we imaged two chicken breast tissue samples (Fig. 3). The samples were prepared with 3.2- and 3-mm radii of curvature, respectively, in the cylindrical bumps. Two objects, shown in Figs. 3(b) and 3(d), were made from 100-μm-thick black latex and placed in the centers of curvature of the prepared samples, i.e., 3.2 and 3 mm below their respective surfaces. Their wide sides were parallel to the ultrasound beam and perpendicular to the light beam. We took the difference between the profiles of the modulated
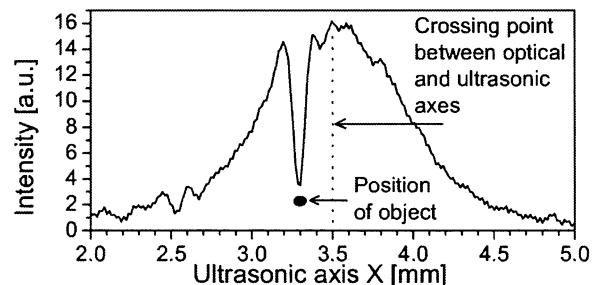
Fig. 2. Temporal dependence of the ultrasound-modulated light intensity during the propagation of an ultrasound pulse through the sample.
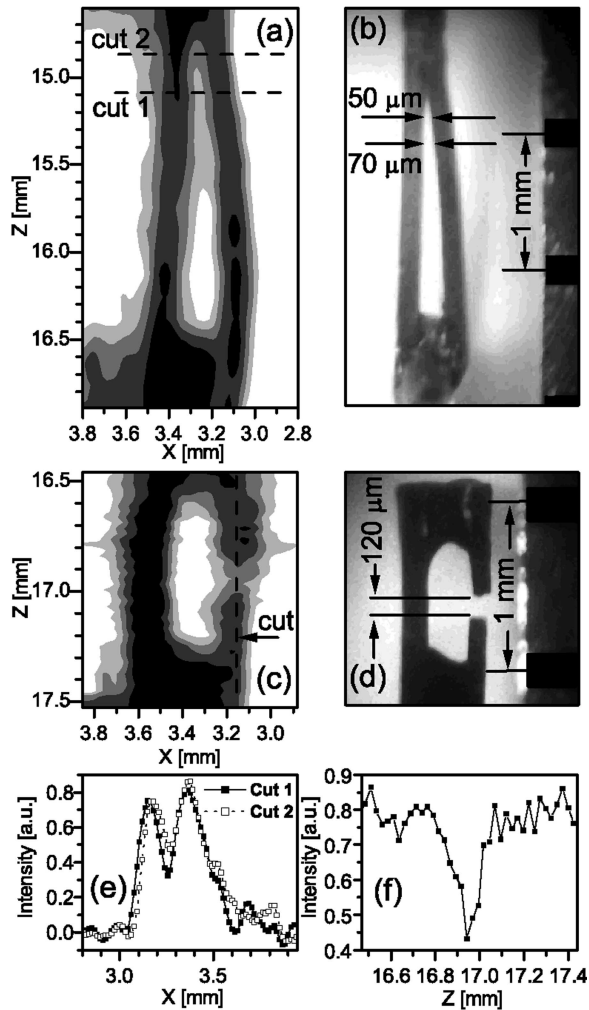
Fig. 3. Measurement of the axial and lateral resolutions. (a) Measurement and (b) image of an object, showing the axial resolution. (c) Measurement and (d) image of an object, showing the lateral resolution. (e) 1D axial profiles of intensity from the data in (a). (f) 1D lateral profile of intensity from the data in (c).

intensity along the X axis and the typical profile without objects present and, subsequently, divided the difference by the latter profile point by point to obtain the relative profiles, which are shown as gray-scale images with five equally spaced gray levels from 0 to 1 [Figs. 3(a) and 3(c)]. Figure 3(e) presents the 1D axial intensity profiles along the X axis taken from the image in Fig. 3(a) at positions $Z = 15.11$ mm and $Z = 14.86$ mm, with an arbitrary origin. At position $Z = 15.11$ mm, the gap had an actual width of only 70 μm along the X axis and was resolved with 55% contrast. When the gap size was reduced to 50 μm at $Z = 14.86$ mm, the contrast decreased to 40%.

Similarly, Fig. 3(f) presents the 1D lateral intensity profile along the Z axis taken from the image in Fig. 3(c) at $X = 3.17$ mm. The gap had an actual width of 120 μm along the Z axis and was resolved with a 50% contrast. If we use the minimal sizes of the resolvable gaps at 50% contrast as the resolutions, the estimated axial and lateral resolutions are 70 and 120 μm, respectively. However, the ultimate resolvable gap sizes at minimal contrast should be much smaller.

In summary, this study has demonstrated the feasibility of high-resolution ultrasound-modulated optical tomography in biological tissue with an imaging depth of several millimeters. A CFPI was shown to be able to isolate ultrasonically modulated light from the background efficiently in real time. The resolution can be further improved by use of higher ultrasound frequencies. This technology can easily be integrated with conventional ultrasound imaging to provide complementary information.

References

1. F. A. Marks, H. W. Tomlinson, and G. W. Brooksby, Proc. SPIE **1888,** 500 (1993).
2. L.-H. V. Wang, S. L. Jacques, and X. Zhao, Opt. Lett. **20,** 629 (1995).
3. W. Leutz and G. Maret, Physica B **204,** 14 (1995).
4. L.-H. V. Wang, Phys. Rev. Lett. **87,** 043903 (2001).
5. S. Sakadžić and L.-H. V. Wang, Phys. Rev. E **66,** 026603 (2002).
6. M. Kempe, M. Larionov, D. Zaslavsky, and A. Z. Genack, J. Opt. Soc. Am. A **14,** 1151 (1997).
7. L.-H. V. Wang and G. Ku, Opt. Lett. **23,** 975 (1998).
8. S. Leveque, A. C. Boccara, M. Lebec, and H. Saint-Jalmes, Opt. Lett. **24,** 181 (1999).
9. G. Yao, S.-L. Jiao, and L.-H. V. Wang, Opt. Lett. **25,** 734 (2000).
10. A. Lev, Z. Kotler, and B. G. Sfez, Opt. Lett. **25,** 378 (2000).
11. M. Hisaka, T. Sugiura, and S. Kawata, J. Opt. Soc. Am. A **18,** 1531 (2001).
12. J. Li, G. Ku, and L.-H. V. Wang, Appl. Opt. **41,** 6030 (2002).
13. A. Lev and B. G. Sfez, Opt. Lett. **28,** 1549 (2003).
14. M. Gross, P. Goy, and M. Al-Koussa, Opt. Lett. **28,** 2482 (2003).
15. J. Li and L.-H. V. Wang, Appl. Phys. Lett. **84,** 1597 (2004).
16. J.-P. Monchalin, Appl. Phys. Lett. **47,** 14 (1985).
17. American Institute of Ultrasound in Medicine, "Mammalian *in vivo* ultrasonic biological effects" (1992), http://www.aium.org/.